Vorticle Fluid Simulation
Technical Memo 15-01

Alexis Angelidis*
Pixar Animation Studios

Figure 1: *Left: gas simulation using 2000 vorticles. Right: particles of densities are emitted into the flow. For rendering, the particles density and velocity are splatted into a volume. Vorticles outside of the frustum are simply deleted.*

Abstract

We present a Lagrangian method for simulating incompressible gases in 3 dimensions. Using the vorticity equation with Lagrangian particles, we create, modify and delete vortices of varying size in a manner that handles buoyancy, boundaries, viscosity and collision with deformable objects using monopoles. Our method scales linearly for parallel processing and provides user controls at varying resolutions. We address common problems of particle-based vortex methods, and provide mathematical justification for all terms. All implementation details are provided.

1 Related Work

The Navier-Stokes Equation [Aris 2012] generalizes Newton's second law to continuums and effectively models the motion of gases. Foster and Metaxas [Foster and Metaxas 1997] and Stam [Stam 1999] solve velocity in an Eulerian frame of reference, with velocity stored in a uniformly voxelized grid. De Witt et al. model the advection of gases using the Laplacian eigenvectors as a basis for incompressible flow [De Witt et al. 2012]. The Navier-Stokes Equation can also be modeled in a Lagrangian frame of reference with Smooth Particle Hydrodynamics [Desbrun and Gascuel 1996]. The Vorticity Equation [Cottet and Koumoutsakos 2000] is obtained by applying the curl operator to the Navier-Stokes Equation, and can be solved with a Vortex Method using point samples [Park and Kim 2005; Zhang and Bridson 2014] or filaments [Angelidis et al. 2006]. Elcott et al. take an original approach, and use Kelvin's theorem instead of Navier-Stokes [Elcott et al. 2007].

To model different characteristics at different resolutions, multiple approaches can be combined. Navier-Stokes and Vortex Methods can be combined and applied to a selective range of scales within the same method: Selle et al. advect vorticity carried by points [Selle et al. 2005] and Pfaff et al. advect vorticity carried by sheets [Pfaff et al. 2012]. Kim et al. advect procedurally generated detail [Kim et al. 2008]. Zhang and Bridson use a voxel grid for large distance flow interaction and particles for near flow interaction to solve the Vorticity Equation [Zhang and Bridson 2014].

While it is now widely expected that a practical algorithm must guarantee stability [Stam 1999], scalability in the number of threads is also an imminent requirement for gas simulation algorithms: the work of Gibou and Chohong [Gibou and Min 2012] and McAdams et al. [McAdams et al. 2010] report that the present bottleneck of methods that solve velocity in a voxelized grid is the Poisson equation. By avoiding the Poisson equation, our method avoids the bottleneck altogether. A boost in computing performance improves the creative iteration process.

The motivating application for this work is the animation of gases for Visual Effects. Controlling the motion of a gas presents known challenges: gases usually don't have a well defined surface and often vary dramatically over time. To produce natural looking gases, artists have to tweak the physical parameters of computational models. Expected controls include external forces, buoyancy, rigid and deformable boundaries, and viscosity. Our model provides all of those and more: user controls at arbitrary resolution, constant cost across resolutions, spatially varying resolution, and decoupled resolutions for density, dynamics and boundary conditions. Our contributions are:

- a new basis that accounts for stretching in a stable manner.
- a new model for viscosity that handles isolated particles.
- a new model for buoyancy.
- a new model for deformable boundaries.
- a new model for vortex shedding.

Our paper is organized as follows. In Section 2, we present the equations from which we derive our model. In Section 2.1, we introduce our vorticle basis. In Section 2.2, we present our vorticity stretching technique. In Section 2.3, we present our viscosity model that handles isolated particles. In Section 2.4, we present our buoyancy model. In Section 2.5, we define the pressure field for boundaries. In Section 2.6 we present our model for vortex shedding. In Section 3, we present our acceleration data structure, followed by an overview of controls in Section 4 and algorithm summary in Section 5.

Our method is implicitly incompressible as is inherent to vortex methods, and does not require enforcing incompressibility by solving a compressible pressure term. The dynamics resolution is de-

*e-mail:silex@pixar.com

coupled from the advected density resolution, thus the density resolution can be modified while preserving the motion. Our method is purely Lagrangian with local dynamic interaction, therefore managing the simulation domain is as simple as managing points. Our most costly step is a point cloud query.

2 Dynamic Model

To obtain our equation of motion, we apply the curl operator to both sides of the following form of the Navier-Stokes Equation of a viscous incompressible Newtonian fluid, divide both sides by ρ, and replace $\frac{\nabla\rho}{\rho}$ with $\nabla\log(\rho)$

$$\rho\frac{\mathrm{d}\vec{\mathbf{v}}}{\mathrm{d}t} = \mu\nabla^2\vec{\mathbf{v}} + \rho\vec{\mathbf{F}} - \nabla p \tag{1}$$

We obtain the following equation that we solve for motion, where the vorticity $\vec{\omega}$ is defined as the curl of the velocity $\vec{\mathbf{v}}$.

$$\frac{\mathrm{d}\vec{\omega}}{\mathrm{d}t} = (\vec{\omega}\cdot\nabla)\vec{\mathbf{v}} + \frac{\mu}{\rho}\nabla^2\vec{\omega} + \nabla\log(\rho)\times(\vec{\mathbf{F}} - \frac{\mathrm{d}\vec{\mathbf{v}}}{\mathrm{d}t}) + \nabla\times\vec{\mathbf{F}} \tag{2}$$

Eq. (2) means that the vorticity $\vec{\omega}$ evolves over time by advecting a Lagrangian frame of reference (particle) that carry $\vec{\omega}$, and stretching $\vec{\omega}$ according to the velocity $\vec{\mathbf{v}}$, with dynamic viscosity μ, buoyancy and boundary interaction specified by density ρ and external forces $\vec{\mathbf{F}}$

$$\vec{\mathbf{F}}(\mathbf{p}) = \begin{cases} \vec{\mathbf{g}} + \vec{\mathbf{e}} & \text{if } \mathbf{p} \text{ outside solid objects} \\ \vec{\mathbf{f}} & \text{otherwise} \end{cases} \tag{3}$$

where $\vec{\mathbf{g}}$ is the constant for gravity, $\vec{\mathbf{f}}$ is the acceleration at the objects' boundaries suitable for deformable objects, and $\vec{\mathbf{e}}$ is user defined external forces. The density is assumed strictly greater than 0. The velocity $\vec{\mathbf{v}}$ is needed for advection, and is obtained from $\vec{\omega}$ by inverting the curl operator with the Biot-Savart law and an irrotational and solenoidal field $\vec{\mathbf{h}}$

$$\begin{aligned} \vec{\mathbf{u}}(\mathbf{p}) &= \tfrac{1}{4\pi}\int_{\mathbf{x}\in\mathbb{R}^3} \tfrac{\vec{\omega}(\mathbf{x})\times(\mathbf{p}-\mathbf{x})}{\|\mathbf{p}-\mathbf{x}\|^3}\mathrm{d}\mathbf{x} \\ \vec{\mathbf{v}} &= \vec{\mathbf{u}} + \vec{\mathbf{h}} \end{aligned} \tag{4}$$

Eq. (4) means that the flow $\vec{\mathbf{v}}$ is the sum of the velocity induced by a continuum of rotations of center $\mathbf{x}$, axis $\vec{\omega}$ and angle $\|\vec{\omega}\|/\|\mathbf{p}-\mathbf{x}\|^3$, with a pressure field $\vec{\mathbf{h}}$ that models the boundary condition. The relation between $\vec{\mathbf{h}}$ and $\vec{\mathbf{f}}$ is given by Eq. (20) and the topic of Section 2.5. Our nomenclature is provided in Appendix A.

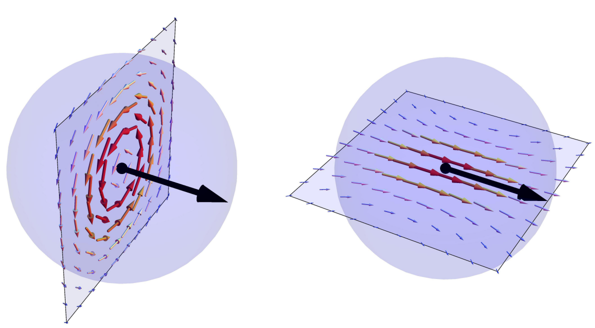

Figure 2: *Left: slice of the velocity field induced by a vorticle. Right: slice of the vorticity field induced by a vorticle.*

2.1 Vorticle and Stretchable Vorticle

This section introduces our basis. We keep the integral inside our discretization of Eq. (4), and introduce with Eq. (5) a vorticle partitioning $(V_i, \vec{\omega}_i)$ where $\vec{\omega}_i$ denotes the vorticity field induced by vorticle i

$$\vec{\mathbf{u}}(\mathbf{p}) = \frac{1}{4\pi}\sum_i \int_{\mathbf{x}\in V_i} \frac{\vec{\omega}_i(\mathbf{x})\times(\mathbf{p}-\mathbf{x})}{\|\mathbf{p}-\mathbf{x}\|^3}\mathrm{d}\mathbf{x} \tag{5}$$

The singularity of Eq. (5) at $\mathbf{p} = \mathbf{x}$ could be removed by integrating analytically the vorticity over the partition or with a regularizing constant. To avoid this laborious integral and avoid an arbitrary post-simulation blurring filter size, we define instead the vorticity field as the sum of the curl of the vorticle's velocity field, as shown in Figure 2, in contrast with other methods that define vorticity as interpolated from point values. This guarantees a divergence free vorticity and avoids instability from vorticity compression. A vorticle is a vorticity particle defined by rotation strength $\vec{\mathbf{w}}_i$, center $\mathbf{x}_i$ and falloff $\phi_i(\mathbf{p})$. The velocity and vorticity fields induced by a vorticle are shown in Figure 2 and given by

$$\vec{\mathbf{v}}_i(\mathbf{p}) = \phi_i\,\vec{\mathbf{w}}_i\times(\mathbf{p}-\mathbf{x}_i) \tag{6a}$$
$$\vec{\omega}_i(\mathbf{p}) = 2\phi_i\vec{\mathbf{w}}_i + \nabla\phi_i\times(\vec{\mathbf{w}}_i\times(\mathbf{p}-\mathbf{x}_i)) \tag{6b}$$

The falloff of a stretchable vorticle $\phi_i = s_i r_i^{-5/2}(1 + \frac{\|\mu_i((\mathbf{p}-\mathbf{x}_i)/r_i)\|^2}{2})^{-3/2}$ and its gradient $\nabla\phi_i$ are centered at $\mathbf{x}_i$, where r_i is the vorticle's size, s_i is the stretching factor, and μ_i is the stretching function $\mu_i(\mathbf{q}) = \frac{1}{\vec{\mathbf{w}}_i^2}(s_i^{-4/5}(\vec{\mathbf{w}}_i\cdot\mathbf{q})\,\vec{\mathbf{w}}_i + s_i^{7/10}\vec{\mathbf{w}}_i\times\mathbf{q}\times\vec{\mathbf{w}}_i)$. The following properties are satisfied by ϕ_i. First, ϕ_i revolves around $\vec{\mathbf{w}}_i$, and therefore $\vec{\mathbf{v}}_i$ is divergence-free since its magnitude is constant along the streamlines of the rotation. Second, when the stretching factor is increased from s_i to s'_i, the vorticity $\vec{\omega}_i$ is stretched by a factor s'_i/s_i along $\vec{\mathbf{w}}_i$ and squashed by $\sqrt{s_i/s'_i}$ along any direction perpendicular to $\vec{\mathbf{w}}_i$, in accordance with the deformation induced by an incompressible flow, and satisfying Kelvin's circulation theorem. Third, stretching is conservative since the vorticle's mean energy E_i is independent of s_i

$$E_i = \frac{1}{2}\int \vec{\mathbf{v}}_i^2\mathrm{d}\mathbf{x} = \sqrt{2}\pi^2\|\vec{\mathbf{w}}_i\|^2 \tag{7}$$

A stretchable vorticle is thus defined by 4 variables $\{\mathbf{x}_i, \vec{\mathbf{w}}_i, r_i, s_i\}$, and we show in the next section how to handle s_i and reduce it to a vorticle of 3 variables

$$\{\mathbf{x}_i, \vec{\mathbf{w}}_i, r_i\} \tag{8}$$

The velocity field is defined by summing the velocity field of multiple vorticles, as shown in Figure 3.

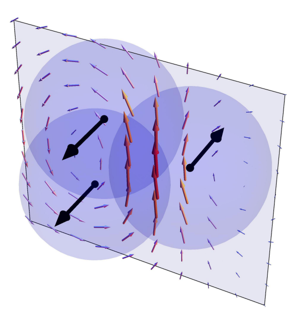

Figure 3: *A velocity field is induced by multiple vorticles, illustrated with three vorticles orthogonal to a plane.*

2.2 Stretching

The term $(\vec{\boldsymbol{\omega}} \cdot \nabla)\vec{\mathbf{v}}$ in Eq. (2) models the stretching of vorticity. We measure stretching at $\mathbf{x}_i$ by applying the velocity gradient to $\vec{\boldsymbol{\omega}}_i(\mathbf{x}_i) = 2r_i^{-5/2}\vec{\mathbf{w}}_i$, the self-induced vorticity at the center of an unstretched vorticle. We obtain

$$\frac{\mathrm{d}\vec{\boldsymbol{\omega}}_i}{\mathrm{dt}}(\mathbf{x}_i) = \sum_j \vec{\mathbf{w}}_j \times \Big(\nabla\phi_j(\mathbf{x}_i)\cdot\vec{\boldsymbol{\omega}}_i(\mathbf{x}_i)(\mathbf{x}_i - \mathbf{x}_j) + \phi_j(\mathbf{x}_i)\vec{\boldsymbol{\omega}}_i(\mathbf{x}_i)\Big) \tag{9}$$

Stretching produces a rotation of $\vec{\mathbf{w}}_i$ and scale of s_i. Let us call $\vec{\boldsymbol{\omega}}_i' = \vec{\boldsymbol{\omega}}_i + D_t\frac{\mathrm{d}\vec{\boldsymbol{\omega}}_i}{\mathrm{dt}}$. The new rotation strength and stretch factor are:

$$\vec{\mathbf{w}}_i' = \|\vec{\mathbf{w}}_i\|\frac{\vec{\boldsymbol{\omega}}_i'}{\|\vec{\boldsymbol{\omega}}_i'\|} \tag{10}$$

$$s_i' = \frac{\|\vec{\boldsymbol{\omega}}_i'\|}{\|\vec{\boldsymbol{\omega}}_i\|} \tag{11}$$

The accumulation of stretching introduces increasingly high frequency velocities by transferring large scale eddies to smaller scale eddies [Frisch and Kolmogorov 1995]. Although the diffusion of Section 2.3 filters eddies over long enough periods of time, instability is not an option and high frequency eddies must be filtered explicitly in a predictable manner. We filter by unstretching the stretchable vorticle in a manner that preserves both E_i and the enstrophy Ω_i of the stretched vorticle

$$\Omega_i = \frac{1}{2}\int \vec{\boldsymbol{\omega}}_i^2\mathrm{d}\mathbf{x} = \frac{3\pi^2(1+4s_i'^3)}{16\sqrt{2}r_i^2 s_i'^{8/5}}\|\vec{\mathbf{w}}_i\|^2 \tag{12}$$

Preserving E_i is trivial since E_i is independent of s_i and r_i in Eq. (7). To preserve Ω_i, we adjust r_i to a new size r_i'

$$r_i' = r_i\ s_i'^{4/5}\sqrt{\frac{5}{1+4s_i'^3}} \tag{13}$$

With Eq. (13) the stretching factor can be restored to 1. This is illustrated in Figure 4. The reader can verify that swapping $\{r_i, s_i'\}$ for $\{r_i', 1\}$ preserves Ω_i. This step is a resampling step, where we use the same vorticle locations. Note that resampling introduces an error, especially when squashing i.e. the stretching factor is below 1. Therefore if taking substeps, we recommend unstretching on full frames to avoid overfiltering. We also set limit resolutions with a lower threshold $r_{\min}$ and upper threshold $r_{\max}$ on the vorticle size r_i. This limit resolution loses enstrophy, but does not lose energy because of Eq. (7). Thus Eq. (10), Eq. (11) and Eq. (13) provide the way to apply stretching to a vorticle. The falloff and falloff gradient for an unstretched vorticle are

$$\begin{aligned} \phi_i &= \sqrt{r_i}(r_i^2 + \tfrac{\|\mathbf{p}-\mathbf{x}_i\|^2}{2})^{-3/2} \\ \nabla\phi_i &= -\tfrac{3}{2}\sqrt{r_i}(r_i^2 + \tfrac{\|\mathbf{p}-\mathbf{x}_i\|^2}{2})^{-5/2}\,(\mathbf{p}-\mathbf{x}_i) \end{aligned} \tag{14}$$

When a vorticle becomes too small and approaches the fluid's Kolmogorov length, viscous forces dominate, and the vorticle strength is dissipated with $\vec{\mathbf{w}}_i' = k\vec{\mathbf{w}}_i$.

2.3 Viscosity

The term $\frac{\mu}{\rho}\nabla^2\vec{\boldsymbol{\omega}}$ in Eq. (2) is the diffusion of vorticity, and models viscosity. We approximate $\frac{\mu}{\rho}$ with a constant kinematic viscosity ν, and derive our viscous model from the modified PSE (particle strength exchange) method described by Cottet and Koumoutsakos [Cottet and Koumoutsakos 2000] which normalizes the discrete integral to avoid a blow up, and we add a term for handling

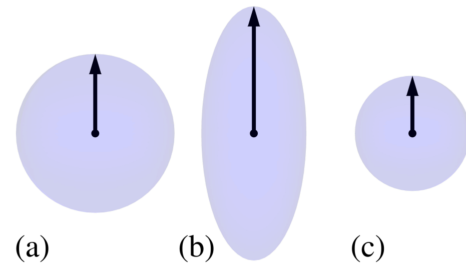

Figure 4: *A vorticle (a) is stretched into vorticle (b): the mean energy is preserved while the enstrophy changes. Vorticle (b) is then resampled in an unstretched vorticle (c) with the same mean energy and enstrophy as vorticle (b).*

isolated particles to model effectively the leakage of vorticity into the region of space with no vorticles. The PSE method is obtained by a Taylor expansion of $\vec{\boldsymbol{\omega}}$, reduced after multiplication with a normalized regularization function η_ϵ. The result of this term is similar to the artificial damping of Park and Kim [Park and Kim 2005], but within the scope of the diffusion

$$\begin{aligned} \frac{\mathrm{d}\vec{\mathbf{w}}_i}{\mathrm{dt}} &= \frac{\nu}{\epsilon^2}((1-\alpha_i)\frac{\sum_j V_j\eta_\epsilon(\mathbf{x}_j-\mathbf{x}_i)(\vec{\mathbf{w}}_j-\vec{\mathbf{w}}_i)}{\sum_j V_j\eta_\epsilon(\mathbf{x}_j-\mathbf{x}_i)} - \alpha_i\vec{\mathbf{w}}_i) \\ \alpha_i &= \prod_{j\neq i}(1-\frac{\eta_\epsilon(\mathbf{x}_j-\mathbf{x}_i)}{\eta_\epsilon(0)}) \end{aligned} \tag{15}$$

where α_i is a measure of the isolation of particle i, η_ϵ is the Gaussian PSE kernel, and V_i is the volume associated with vorticle i

$$\begin{aligned} \eta_\epsilon(\mathbf{x}) &= \frac{1}{\sqrt{2}\epsilon^3\pi^{3/2}}\exp(-\frac{\|\mathbf{x}\|^2}{2\epsilon^2}) \\ V_i &= \int\phi_i\mathrm{d}\mathbf{x} = 2\sqrt{2}\pi^2\sqrt{r_i}s_i^{2/5} \end{aligned} \tag{16}$$

We use $\epsilon = \sqrt{\nu D_t}$, thus making viscosity cheaper for low ν and small time steps. This result can also be interpreted as a convolution with the heat kernel.

2.4 Buoyancy

When $\mathbf{p}$ is outside of solid objects, the term $\nabla\log(\rho)\times(\vec{\mathbf{F}} - \frac{\mathrm{d}\vec{\mathbf{v}}}{\mathrm{dt}}) + \nabla\times\vec{\mathbf{F}}$ in Eq. (2) reduces to $\nabla\log(\rho)\times(\vec{\mathbf{g}}+\vec{\mathbf{e}}-\frac{\mathrm{d}\vec{\mathbf{v}}}{\mathrm{dt}})$, and models the vorticity induced by buoyancy. New vorticles are produced from the density field ρ releasing potential energy, as shown in Figure 5. We define ρ with a set of particles carrying density and an ambient density $\rho_{\mathrm{A}} > 0$, so the total density field ρ is strictly greater than 0, as required by Eq. (2)

$$\rho = \rho_{\mathrm{A}} + \sum \rho_j \tag{17}$$

We use subscript j to denote density particles, as opposed to subscript i for vorticles. The falloff ρ_j of a density particle j is centered at $\mathbf{x}_j$, and defined per Appendix B in local coordinates $\mathbf{q}_j = \mathbf{p} - \mathbf{x}_j$ as

$$\rho_j = m_j\frac{\exp((1+\kappa_1\frac{\mathbf{q}_j\cdot\mathbf{q}_j}{2r_j^2})^{-\kappa_2}) - 1}{\mathrm{e}-1} \tag{18}$$

where m_j is a multiplier of the particle density field, and κ_i is given in Eq. (37). The newly induced vorticles are located along a ring of diameter r_j perpendicular to $\vec{\mathbf{g}}+\vec{\mathbf{e}}-\frac{\mathrm{d}\vec{\mathbf{v}}}{\mathrm{dt}}$. Instead of advecting an additional filament representation, we discretize the ring with n new vorticles, equidistant for simplicity, and where $n = 2$ in practice. Let us define orthogonal unit vectors $\vec{\mathbf{a}}$ and $\vec{\mathbf{b}}$ such that $\vec{\mathbf{a}}\times\vec{\mathbf{b}}$ has the direction of $\vec{\mathbf{g}}+\vec{\mathbf{e}}-\frac{\mathrm{d}\vec{\mathbf{v}}}{\mathrm{dt}}$. Given n randomly selected samples α_j, the new vorticles are, in the density particle's local coordinates

$$\begin{aligned}
\mathbf{x}_{\alpha_j} &= \mathbf{x}_j + \tfrac{r_j}{2}(\cos(\alpha_j)\vec{\mathbf{a}} + \sin(\alpha_j)\vec{\mathbf{b}}) \\
\vec{\mathbf{w}}_{\alpha_j} &= r_j\sqrt{r_j}\kappa_0 \tfrac{\pi}{n}\|\vec{\mathbf{g}} + \vec{\mathbf{e}} - \tfrac{\mathrm{d}\vec{\mathbf{v}}}{\mathrm{dt}}\| \tfrac{\rho_j(\mathbf{x}_\alpha) + \frac{m_j}{\mathrm{e}-1}}{\rho(\mathbf{x}_\alpha)} \\
&\quad (-\sin(\alpha_j)\vec{\mathbf{a}} + \cos(\alpha_j)\vec{\mathbf{b}}) \\
r_{\alpha_j} &= r_j
\end{aligned} \tag{19}$$

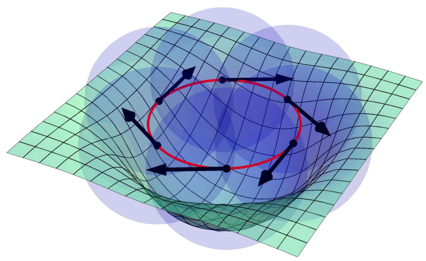

Figure 5: *A density particle emits a ring of vorticles (red). We sample the ring with vorticles of strengths that match the mass of the density particles, as visualized on points (green lattice).*

2.5 Boundary Pressure

In Eq. (4), the field $\vec{\mathbf{h}}$ cancels the velocity field induced by the vorticles without adding vorticity. To define $\vec{\mathbf{h}}$, we split $\mathbb{R}^3$ with a surface $\delta\Omega$ enclosing volume Ω with normal $\vec{\mathbf{n}}$ pointing outside, and volume Ω^c the complementary of Ω. We show in Appendix **C** that the Neumann boundary condition defines $\vec{\mathbf{h}}$ restricted to Ω^c explicitly as

$$\vec{\mathbf{h}}_{\Omega^c}(\mathbf{p}) = \oiint_{\delta\Omega} \vec{\mathbf{n}} \cdot (\vec{\mathbf{v}}_{\Omega^c}(\mathbf{x}) - \vec{\mathbf{u}}(\mathbf{x}))\nabla G(\mathbf{p}, \mathbf{x})\mathrm{d}\mathbf{x} \tag{20}$$

Here $G(\mathbf{p}, \mathbf{x}) = \frac{-1}{4\pi\|\mathbf{p}-\mathbf{x}\|}$ is the Green's function of the Laplacian, $\vec{\mathbf{v}}_{\Omega^c}$ is the velocity of the boundary. To the best of our knowledge, we are not aware of this result in previous work, although this is related to the method of Zhang and Bridson [Zhang and Bridson 2014] who solve $\vec{\mathbf{h}}$ numerically using the single layer potential from Potential theory. Using n panels of size a_i and centroid $\mathbf{x}_i$, we could discretize $\vec{\mathbf{h}}$ using directly the falloffs

$$\vec{\mathbf{h}}_{\Omega^c}(\mathbf{p}) = \sum_i a_i\vec{\mathbf{n}}_i \cdot (\vec{\mathbf{v}}_{\Omega^c}(\mathbf{x}_i) - \vec{\mathbf{u}}(\mathbf{x}_i))\nabla G(\mathbf{p}, \mathbf{x}_i) \tag{21}$$

To avoid the singularities of G when $\mathbf{p}$ approaches the boundary samples $\mathbf{x}_i$, we use, instead of Eq. (21), the pathlines of the monopole based on the deformer of Decaudin [Decaudin 1996]. For a point outside of the boundary

$$\vec{\mathbf{h}}_{\Omega^c}(\mathbf{p}) = \frac{1}{D_t}\sum_i \zeta(\mathbf{p}-\mathbf{x}_i, D_t a_i \vec{\mathbf{n}}_i \cdot (\vec{\mathbf{v}}_{\Omega^c}(\mathbf{x}_i) - \vec{\mathbf{u}}(\mathbf{x}_i))) - (\mathbf{p}-\mathbf{x}_i) \tag{22}$$

where ζ defined below satisfies $\zeta(\zeta(\mathbf{p}, k_0), k_1) = \zeta(\mathbf{p}, k_0 + k_1)$

$$\begin{aligned}
\zeta(\mathbf{p}, k) &= \begin{cases} (1 + \frac{3\ k}{4\pi\|\mathbf{p}\|^3})^{1/3}\ \mathbf{p}\ \text{ if } r(k) < \|\mathbf{p}\| \\ 0 \text{ otherwise} \end{cases} \\
r(k) &= (\max(-k, 0)\tfrac{3}{4\pi})^{1/3}
\end{aligned} \tag{23}$$

This provides a geometric insight: a boundary opposing the flow is akin to an insertion and removal of volume at the boundary proportional to the boundary's opposition to the flow. The discretization of $\vec{\mathbf{h}}$ is stable, but more accurate away from the boundary than near the boundary. To remedy the problem of accuracy, we define the solution $\vec{\mathbf{h}}_{\delta\Omega}$ on the boundary. Since $\vec{\mathbf{n}} \cdot \vec{\mathbf{h}}_{\delta\Omega} = \vec{\mathbf{n}} \cdot (\vec{\mathbf{v}}_{\Omega^c} - \vec{\mathbf{u}})$ and $\vec{\mathbf{h}}_{\delta\Omega}$ is aligned with the normal

$$\vec{\mathbf{h}}_{\delta\Omega}(\mathbf{p}) = (\vec{\mathbf{n}} \cdot (\vec{\mathbf{v}}_{\Omega^c}(\mathbf{p}) - \vec{\mathbf{u}}(\mathbf{p})))\,\vec{\mathbf{n}} \tag{24}$$

And finally, if a point $\mathbf{p}$ enters the boundary, it is pushed out to the nearest position on the surface

$$\vec{\mathbf{h}}_{\Omega}(\mathbf{p}) = \underset{\mathbf{x}\in\delta\Omega}{\operatorname{argmin}}(\|\mathbf{p} - \mathbf{x}\|) \tag{25}$$

We assemble Eq. (22), Eq. (24) and Eq. (25) to construct the full definition of $\vec{\mathbf{h}}$, by blending $\vec{\mathbf{h}}_{\Omega^c}$ and $\vec{\mathbf{h}}_{\delta\Omega}$ with a smoothstep function based on the distance $\hat{r}$ between the samples on the boundary

$$\vec{\mathbf{h}}(\mathbf{p}) = \begin{cases} \vec{\mathbf{h}}_{\Omega}(\mathbf{p}) \text{ if } \mathbf{p} \in \Omega \\ \mathrm{mix}(\vec{\mathbf{h}}_{\delta\Omega}(\mathbf{p}), \vec{\mathbf{h}}_{\Omega^c}(\mathbf{p})) \text{ otherwise} \end{cases} \tag{26}$$

Where $\mathrm{mix}(\vec{\mathbf{a}}, \vec{\mathbf{b}}) = \vec{\mathbf{a}} + \mathrm{smoothstep}(\frac{d}{\hat{r}})(\vec{\mathbf{b}} - \vec{\mathbf{a}})$, given the distance d from $\mathbf{p}$ to $\delta\Omega$.

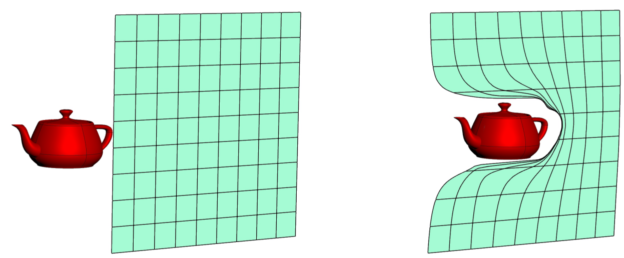

Figure 6: *Left: initial position of a boundary object (red) moving into points (green lattice). Right: the harmonic field warps space in an incompressible and irrotational manner, with a slip boundary.*

2.6 Vorticle Shedding

When $\mathbf{p}$ is at the boundary of a solid object, the term $\nabla\log(\rho) \times (\vec{\mathbf{F}} - \frac{\mathrm{d}\vec{\mathbf{v}}}{\mathrm{dt}}) + \nabla \times \vec{\mathbf{F}}$ in Eq. (2) measures the change of vorticity at the moving object's boundary. This vorticity spreads into the flow by a diffusion proportional to viscosity coefficient ν introduced in Section 2.3. We show in Appendix **D** that the surface vorticity that satisfies our boundary conditions is $(\vec{\mathbf{f}} - \vec{\mathbf{e}} - \frac{\mathrm{d}\vec{\mathbf{v}}}{\mathrm{dt}}) \times \vec{\mathbf{n}}$. The vorticity shedding is the solution to a differential equation with boundary condition

$$\begin{cases} \frac{\mathrm{d}\vec{\boldsymbol{\omega}}}{\mathrm{dt}} = \nu\nabla^2\vec{\boldsymbol{\omega}} \\ \vec{\boldsymbol{\omega}} \underset{\mathbf{p}\in\Omega}{=} D_t\,(\vec{\mathbf{f}} - \vec{\mathbf{e}} - \frac{\mathrm{d}\vec{\mathbf{v}}}{\mathrm{dt}}) \times \vec{\mathbf{n}} \end{cases} \tag{27}$$

We solve Eq. (27) by shedding vorticles: we divide the surface into n panels of area a_i and centroid $\mathbf{x}_i$, and emit per panel a vorticle that approximates the heat kernel

$$\begin{aligned}
\vec{\mathbf{w}}_i &= a_i \tfrac{r^{5/2}}{8\pi D_t \nu}(\vec{\mathbf{f}} - \vec{\mathbf{e}} - \tfrac{\mathrm{d}\vec{\mathbf{v}}}{\mathrm{dt}}) \times \vec{\mathbf{n}} \\
r_i &= \sqrt{2}\sqrt{D_t\,\nu}
\end{aligned} \tag{28}$$

We use $\|(\vec{\mathbf{f}} - \vec{\mathbf{e}} - \frac{\mathrm{d}\vec{\mathbf{v}}}{\mathrm{dt}}) \times \vec{\mathbf{n}}\|$ as a probability distribution function to create samples at the locations that most affect the flow. Note that $\vec{\mathbf{f}}$ is the surface acceleration, as opposed to the velocity. To compute the acceleration, we store on the surface Eq. (4) at the previous time, and use $\frac{\mathrm{d}\vec{\mathbf{v}}}{\mathrm{dt}} \simeq \frac{\vec{\mathbf{v}}(t) - \vec{\mathbf{v}}(t-D_t)}{D_t}$. We show in Figure 7 that this produces the expected behavior.

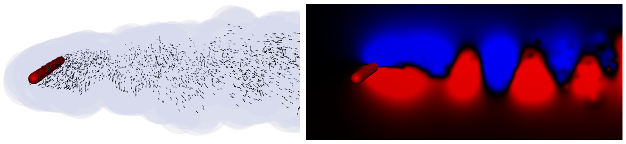

Figure 7: *Left: a constant flow moves at $10ms^{-1}$ with $\nu = 0.1$ around a static pole of radius 1 (red): the surface sheds vorticles (black arrows). Right: a slice of the vorticity induced by the vorticles reveals the emergent behavior of a von Kármán vortex street.*

3 Data Structure

For efficiency, we introduce a vorticle cutoff proportional to the vorticle size r_i. This reduces the algorithmic complexity to $\mathcal{O}(N)$ when neighbor cell lists are used. This accelerates the nearest vorticle search while preserving an incompressible flow since the cutoff is constant along the streamlines of rotation. Since vorticles are band limited, we can further split the vorticles into groups of similar radius, and evaluate their displacement in sparse grids with cell size proportional to the cutoff.

Vorticle cutoff We introduce the cutoff on both the falloff and its gradient in a manner that preserves smoothness. Let us define a vorticle's cutoff distance mr_i. Using the following values

$$\begin{aligned} k_0 &= 4(1+2m^2)r_i \\ k_1 &= 2+m^2 \\ k_2 &= k_1^2\sqrt{k_1} \\ a_0 &= \frac{r_i}{r_i-\sqrt{2k_0/k_2}} \\ a_1 &= \sqrt{2}\,\frac{k_0-6m\|\mathbf{p}-\mathbf{x}_i\|}{k_2\sqrt{r_i}r_i^3} \\ a_3 &= \frac{6\sqrt{2}}{k_2\sqrt{r_i}r_i^4} \end{aligned} \tag{29}$$

Then the remapped falloff and gradient are

$$\begin{aligned} \tilde{\phi}_i &= a_0(\phi_i - a_1) \\ \nabla\tilde{\phi}_i &= \nabla\phi_i + a_3(\mathbf{p}-\mathbf{x}_i) \end{aligned} \tag{30}$$

The vorticle cutoff provides an adjustable tradeoff between the falloff's physically based properties and spatially localized computations, with defaults typically set to $6r_i$ and $r_i/2$.

Fusing vorticles Vorticles that are similar and close enough can be fused in one vorticle. Vorticle are similar enough when $\|\mathbf{p}_i - \mathbf{p}_j\|$ and $|r_i - r_j|$ are smaller than a distance threshold ϵ. Also, the velocity induced by a group of far away vorticles can be obtained by fusing the vorticles. The fused vorticle is given by the following formula

$$\begin{aligned} \mathbf{x} &= \frac{\sum \mathbf{x}_i}{n} \\ r &= \left(\frac{\sum_i r_i^{-5/2}}{\sum_i \sqrt{r_i}}\right)^{-1/3} \\ \vec{\mathbf{w}} &= \frac{\sum_i \sqrt{r_i}\vec{\mathbf{w}}_i}{\sqrt{r}} \end{aligned} \tag{31}$$

where n is the number of vorticles in the cell and i is the vorticle index. The above is asymptotic to the sum of vorticles, and exactly equal to the sum when the vorticles have the same radius.

Lifespan Vorticles can be assigned an artificial decay rate, triggered by an event controlled by a varying expression.

Band-limiting As stretching deforms vorticles outside of the range $(r_{\min}, r_{\max})$, we reduce the vorticle's strength $\vec{\mathbf{w}}_j$ instead of scaling the vorticle's radius r_i. For shrinking small vorticles, this models the fluid's viscous behavior at small scales, and for expanding large vorticles this reduces their contribution to velocity artificially.

Radius paging Splitting the vorticles in groups of similar radius leads to a more efficient use of acceleration structure for distance queries. We use a logarithmic scale to split the vorticles in groups.

Cached velocity When the point density is particularly high within a region of space, velocity can be evaluated at the vertices of a lattice and interpolated in-between.

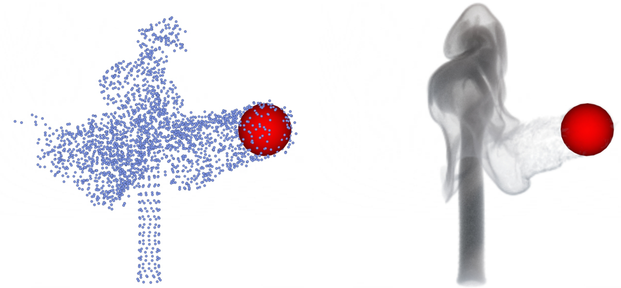

Figure 8: *Left: 2400 vorticles, showing the vertical current and the collider's trail. Right: advected densities. Dynamics can be limited to the visible areas simply by deleting points.*

4 Controls

The number of samples of the colliders, shedding, sources, buoyancy and density are controlled independently. Users can control the flow by modifying existing vorticles with external forces $\vec{\mathbf{e}}$ or via the harmonic field $\vec{\mathbf{h}}$, or by creating new vorticles:

- A turbulent field is created by scattering vorticles with random parameters.
- A gust of wind is created by placing vorticles aligned with the tangent of a ring perpendicular to the direction of the desired wind.
- An invisible collider can be moved to warp space.
- The amount of shedding and buoyancy can be artificially dialed up or down.

A number of additional dials can be tuned per vorticle:

Overshoot For advection of visible particles, the velocity can be scaled lower or higher to create a drag or extra swirliness. Although physically implausible, this helps creating styles.

Spin The axis of vorticles can be aligned with vector fields to modify the fluid motion globally.

Artificial damping The strength of vorticles can be reduced artificially. This damping coefficient can be stored per vorticle.

5 Algorithm Summary

In this section we summarize our algorithm. Several integration schemes may be used to advect particles along the induced velocity field. A simple method, very stable for large time steps, relies on the well understood circular pathlines of individual vorticles, and we replace Eq. (6a) with

$$\begin{aligned}\vec{\mathbf{k}}_w &= D_t\phi_i(\mathbf{p}-\mathbf{x}_i)\vec{\mathbf{w}}_i\\ \vec{\mathbf{k}}_x &= \vec{\mathbf{k}}_w\times(\mathbf{p}-\mathbf{x}_i)\\ \vec{\mathbf{v}}_i(\mathbf{p}) &= \tfrac{1}{D_t}\big(\tfrac{1-\cos(\|\vec{\mathbf{k}}_w\|)}{\vec{\mathbf{k}}_w^2}\vec{\mathbf{k}}_w\times\vec{\mathbf{k}}_x+\tfrac{\sin(\|\vec{\mathbf{k}}_w\|)}{\|\vec{\mathbf{k}}_w\|}\vec{\mathbf{k}}_x\big)\end{aligned} \tag{32}$$

In the following we distinguish between density particles for buoyancy, vorticles for dynamics, and visual particles for rendering.

- Scatter point samples on boundaries using the probability distribution of Section 2.6.
- Compute and store the velocity $\vec{\mathbf{u}}$ induced by vorticles on boundary point samples using Eq. (4).
- Create new vorticles from vortex shedding, defined by Eq. (28) of Section 2.6.
- Create new vorticles from buoyancy, defined by Eq. (19) of Section 2.4.
- Emit new vorticles as defined by the user. Scattering vorticles produces an initial condition. Emitting vorticles on a circle with tangential strength produces a source of wind.
- Build a hierarchy by fusing vorticles, to accelerate evaluating the velocity induced by groups of distant vorticles.
- Compute and store the velocity $\vec{\mathbf{h}}$ induced by colliders on the visual particles using Eq. (26) of Section 2.5. Compute and store the velocity $\vec{\mathbf{u}}$ induced by vorticles on the visual particles using Eq. (4).
- Compute and store the velocity $\vec{\mathbf{h}}$ induced by colliders on the density particles using Eq. (26) of Section 2.5. Compute and store the velocity $\vec{\mathbf{u}}$ induced by vorticles on the density particles using Eq. (4).
- Compute and store the velocity $\vec{\mathbf{h}}$ induced by colliders on the vorticles using Eq. (26) of Section 2.5. Compute and store the velocity $\vec{\mathbf{u}}$ induced by vorticles on the vorticles using Eq. (4).
- Apply displacement $D_t(\vec{\mathbf{u}}+\vec{\mathbf{h}})$ to visual particles, density particles and vorticles.
- Fuse vorticles that can be fused using Eq. (31).
- Attenuate vorticles.
- Delete vorticles far from visual particles, outside of frustum, or with a low strength.

6 Conclusion

We presented a method for simulating gases using vorticles. Our method has no divergence by construction and avoids solving pressure completely. The simulation is gridless and can span domains of arbitrary size and resolution. The sampling resolution of density, dynamics, boundary condition and sources are decoupled from each other, which opens many options for adaptive sampling strategies. Although our method is similar to other point-based vortex methods, a subtle difference is that instead of filtering a point vorticity, we advect vorticles that carry a volume of vorticity. This leads to stable stretching. Additional stability is achieved by integrating streamlines instead of velocity. Also, we propose a model for boundary pressure that does not require solving a linear system, and we propose a model for buoyancy which plays a key role in gas motion for producing more lively smokes and pyroclastic effects. Our method provides a full set of features expected from a gas simulation while using only vorticles and monopoles, and was used on a production. We believe that defining a vorticle in relation to the Navier-Stokes equation provides a valuable insight for future research in vorticity based dynamics.

A Nomenclature

t	time	D_t	time step
$\mathbf{p}$	position	$\mathbf{x}_i$	vorticle center
$\vec{\mathbf{v}}$	velocity	$\vec{\mathbf{v}}_i$	vorticle velocity
$\vec{\boldsymbol{\omega}}$	vorticity	$\vec{\boldsymbol{\omega}}_i$	vorticle vorticity
$\vec{\mathbf{w}}_i$	vorticle strength	r_i	vorticle size
s_i	vorticle stretching factor	$\vec{\mathbf{h}}$	harmonic field
ρ	density	ρ_A	ambient density
ρ_j	particle density	m_j	particle density multiplier
ν	kinematic viscosity	μ	dynamic viscosity
E_i	vorticle mean energy	Ω_i	vorticle enstrophy
$\vec{\mathbf{F}}$	external forces	$\vec{\mathbf{f}}$	solid objects acceleration
$\vec{\mathbf{g}}$	gravity	$\delta\Omega$	boundary surface
Ω	space inside boundary	Ω^c	space outside boundary

(33)

B Buoyancy

The vorticity induced by buoyancy could be computed directly by sampling everywhere in $\Re^3$, the buoyancy term with vorticles. But this laborious integral can be avoided, since buoyancy vorticity is concentrated near places of varying density and where the density gradient and buoyant acceleration are perpendicular. First we associate a set of vorticles with a single particle j which we will generalize to multiple density particles. Let us define a local coordinate system centered at $\mathbf{x}_j$ such that $\vec{\mathbf{z}}$ is aligned with $\vec{\mathbf{g}}+\vec{\mathbf{e}}-\frac{\mathrm{d}\vec{\mathbf{v}}}{\mathrm{d}t}$. For a density particle or radius r_j, we expect the vorticles induced by buoyancy to be concentrated around a ring $\{\mathbf{x}_\alpha, \alpha\in 2\pi\}$ of diameter r_j, perpendicular to vector unit $\vec{\mathbf{z}}$, with an axis $\vec{\mathbf{n}}_\alpha$. In local coordinates

$$\begin{aligned}\mathbf{x}_\alpha &= \tfrac{r_j}{2}(\cos(\alpha),\sin(\alpha),0)\\ \vec{\mathbf{n}}_\alpha &= (-\sin(\alpha),\cos(\alpha),0)\end{aligned} \tag{34}$$

For a canonical density particle, we use the following density field

$$\hat{\rho}_j = \exp\big((1+\kappa_1\frac{\mathbf{x}\cdot\mathbf{x}}{2r_j^2})^{-\kappa_2}\big) \tag{35}$$

We fit parameters κ_0, κ_1 and κ_2 using the following equation

$$\begin{aligned}&\nabla\log(\hat{\rho}_j)\times\vec{\mathbf{z}}\\ &\quad= r_j\sqrt{r_j}\kappa_0\,\nabla\times\big(\textstyle\int_\alpha\phi(\mathbf{p}-\mathbf{x}_\alpha)\vec{\mathbf{w}}_\alpha\times(\mathbf{p}-\mathbf{x}_\alpha)\mathrm{d}\alpha\big)\end{aligned} \tag{36}$$

We obtain the following parameters. The left and right side of Eq. (36) are compared in Figure 9

$$\begin{aligned}\kappa_0 &= 0.493483\\ \kappa_1 &= 0.572636\\ \kappa_2 &= 3.423340\end{aligned} \tag{37}$$

To generalize to multiple particles, we remap $\hat{\rho}_j$ to values in $(0, m_j)$ so that densities can be added, and obtain the field of a single particle density $\rho_j = m_j\frac{\hat{\rho}_j-1}{\mathrm{e}-1}$. Since $\frac{\nabla\rho}{\rho}\times\vec{\mathbf{z}} = \sum\frac{m_j}{\mathrm{e}-1}\frac{\hat{\rho}_j}{\rho}\nabla\log(\hat{\rho}_j)\times\vec{\mathbf{z}}$, we obtain a set of weights that modulate the rotations of the vorticles induced by the density particle j, that accounts for acceleration and multiple particles

$$\vec{\mathbf{w}}_\alpha = r_j\sqrt{r_j}\kappa_0\frac{\pi}{n}\|\vec{\mathbf{g}}+\vec{\mathbf{e}}-\frac{\mathrm{d}\vec{\mathbf{v}}}{\mathrm{d}t}\|\frac{m_j}{\mathrm{e}-1}\frac{\hat{\rho}_j(\mathbf{x}_\alpha)}{\rho(\mathbf{x}_\alpha)}\vec{\mathbf{n}}_\alpha \tag{38}$$

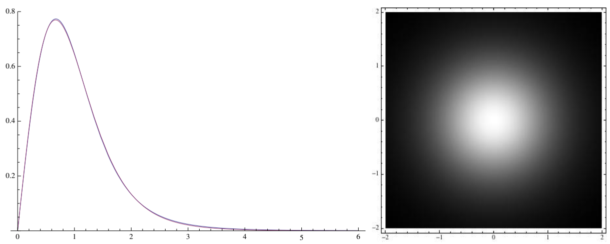

Figure 9: *Left: overlapping plot of the largest component of the left (red) and right (blue) side of Eq. (36). Our density fits the closed form integral with a third decimal accuracy on all 3 vector components. Right: density field ρ_j for $r_j = 1$ and m_j = 1.*

C Boundary Pressure

Let us call G the Green's function of the Laplacian $G(\mathbf{p},\mathbf{x}) = \frac{-1}{4\pi\|\mathbf{p}-\mathbf{x}\|}$. Let us denote $\delta\Omega$ a surface enclosing volume Ω, with normal $\vec{\mathbf{n}}$ pointing outside, and volume Ω^c the complementary of Ω.

Lemma 1 For any vector field $\vec{\mathbf{v}}$ we can define the following irrotational and incompressible vector field $\vec{\mathbf{h}}_{\Omega^c}$, such that $\vec{\mathbf{v}} + \vec{\mathbf{h}}_{\Omega^c}$ does not cross the surface $\delta\Omega$

$$\vec{\mathbf{h}}_{\Omega^c}(\mathbf{p}) = -\oiint_{\delta\Omega} \vec{\mathbf{n}} \cdot \vec{\mathbf{v}}(\mathbf{x}) \nabla G(\mathbf{p},\mathbf{x}) \mathrm{d}\mathbf{x} \tag{39}$$

Proof 1 Using the delta function

$$\delta^3(\mathbf{p}-\mathbf{x}) = \nabla^2 G(\mathbf{p},\mathbf{x}) \tag{40}$$

and using the vector derivative identity

$$\nabla^2 \vec{\mathbf{f}} = \nabla(\nabla \cdot \vec{\mathbf{f}}) - \nabla \times (\nabla \times \vec{\mathbf{f}}) \tag{41}$$

for $\mathbf{p} \in \Omega^c$ we write the Helmholtz decomposition of $\vec{\mathbf{h}}_{\Omega^c}$, as the sum of an irrotational field and solenoidal field

$$\begin{aligned} \vec{\mathbf{h}}_{\Omega^c}(\mathbf{p}) &= \iiint_{\Omega^c} \vec{\mathbf{h}}_{\Omega^c}(\mathbf{x}) \delta^3(\mathbf{p}-\mathbf{x}) \mathrm{d}\mathbf{x} \\ &= \nabla \iiint_{\Omega^c} \nabla \cdot (G(\mathbf{p},\mathbf{x}) \vec{\mathbf{h}}_{\Omega^c}(\mathbf{x})) \mathrm{d}\mathbf{x} \\ &\quad -\nabla \times \iiint_{\Omega^c} \nabla \times (G(\mathbf{p},\mathbf{x}) \vec{\mathbf{h}}_{\Omega^c}(\mathbf{x})) \mathrm{d}\mathbf{x} \\ &= \nabla \iiint_{\Omega^c} \nabla G(\mathbf{p},\mathbf{x}) \cdot \vec{\mathbf{h}}_{\Omega^c}(\mathbf{x}) \mathrm{d}\mathbf{x} \\ &\quad -\nabla \times \iiint_{\Omega^c} \nabla G(\mathbf{p},\mathbf{x}) \times \vec{\mathbf{h}}_{\Omega^c}(\mathbf{x}) \mathrm{d}\mathbf{x} \end{aligned} \tag{42}$$

With derivative notation $\nabla' = \frac{\mathrm{d}}{\mathrm{d}\mathbf{x}}$, we note that $\nabla G(\mathbf{p},\mathbf{x}) = -\nabla' G(\mathbf{p},\mathbf{x})$

$$\begin{aligned} \vec{\mathbf{h}}_{\Omega^c}(\mathbf{p}) &= -\nabla \iiint_{\Omega^c} \nabla' G(\mathbf{p},\mathbf{x}) \cdot \vec{\mathbf{h}}_{\Omega^c}(\mathbf{x}) \mathrm{d}\mathbf{x} \\ &\quad +\nabla \times \iiint_{\Omega^c} \nabla' G(\mathbf{p},\mathbf{x}) \times \vec{\mathbf{h}}_{\Omega^c}(\mathbf{x}) \mathrm{d}\mathbf{x} \end{aligned} \tag{43}$$

Then since $\vec{\mathbf{h}}_{\Omega^c}$ is solenoidal and irrotational we can use identities $\nabla' G \cdot \vec{\mathbf{h}}_{\Omega^c} = \nabla' \cdot (G \vec{\mathbf{h}}_{\Omega^c})$ and $\nabla' G \times \vec{\mathbf{h}}_{\Omega^c} = \nabla' \times (G \vec{\mathbf{h}}_{\Omega^c})$ to write

$$\begin{aligned} \vec{\mathbf{h}}_{\Omega^c}(\mathbf{p}) &= -\nabla \iiint_{\Omega^c} \nabla' \cdot (G(\mathbf{p},\mathbf{x}) \vec{\mathbf{h}}_{\Omega^c}(\mathbf{x})) \mathrm{d}\mathbf{x} \\ &\quad +\nabla \times \iiint_{\Omega^c} \nabla' \times (G(\mathbf{p},\mathbf{x}) \vec{\mathbf{h}}_{\Omega^c}(\mathbf{x})) \mathrm{d}\mathbf{x} \end{aligned} \tag{44}$$

Then using the divergence theorem of the first term, assuming $\vec{\mathbf{n}}$ points outside and the field vanishes faster than $1/r$ as $r \to \infty$

$$\begin{aligned} \vec{\mathbf{h}}_{\Omega^c}(\mathbf{p}) &= \nabla \oiint_{\delta\Omega} \vec{\mathbf{n}} \cdot (G(\mathbf{p},\mathbf{x}) \vec{\mathbf{h}}_{\Omega^c}(\mathbf{x})) \mathrm{d}\mathbf{x} \\ &\quad +\nabla \times \iiint_{\Omega^c} \nabla' \times (G(\mathbf{p},\mathbf{x}) \vec{\mathbf{h}}_{\Omega^c}(\mathbf{x})) \mathrm{d}\mathbf{x} \end{aligned} \tag{45}$$

Field $\vec{\mathbf{h}}_{\Omega^c}$ is irrotational, and if Ω^c is simply connected we can then write $\vec{\mathbf{h}}_{\Omega^c}$ as the gradient of a scalar field, $\vec{\mathbf{h}}_{\Omega^c} = \nabla\chi$. Using the identity $\nabla' \times (G\nabla'\chi) = -\nabla' \times (\chi\nabla' G)$ on the second term

$$\begin{aligned} \vec{\mathbf{h}}_{\Omega^c}(\mathbf{p}) &= \nabla \oiint_{\delta\Omega} \vec{\mathbf{n}} \cdot (G(\mathbf{p},\mathbf{x}) \vec{\mathbf{h}}_{\Omega^c}(\mathbf{x})) \mathrm{d}\mathbf{x} \\ &\quad -\nabla \times \iiint_{\Omega^c} \nabla' \times (\chi(\mathbf{x}) \nabla' G(\mathbf{p},\mathbf{x})) \mathrm{d}\mathbf{x} \end{aligned} \tag{46}$$

Then using the curl theorem of the second term, assuming the field vanishes faster than $1/r$ as $r \to \infty$

$$\begin{aligned} \vec{\mathbf{h}}_{\Omega^c}(\mathbf{p}) &= \nabla \oiint_{\delta\Omega} \vec{\mathbf{n}} \cdot (G(\mathbf{p},\mathbf{x}) \vec{\mathbf{h}}_{\Omega^c}(\mathbf{x})) \mathrm{d}\mathbf{x} \\ &\quad -\nabla \times \oiint_{\delta\Omega} \vec{\mathbf{n}} \times (\chi(\mathbf{x}) \nabla' G(\mathbf{p},\mathbf{x})) \mathrm{d}\mathbf{x} \end{aligned} \tag{47}$$

We apply the gradient to the first term and the curl to the second term

$$\begin{aligned} \vec{\mathbf{h}}_{\Omega^c}(\mathbf{p}) &= \oiint_{\delta\Omega} \vec{\mathbf{n}} \cdot \vec{\mathbf{h}}_{\Omega^c}(\mathbf{x}) \nabla G(\mathbf{p},\mathbf{x}) \mathrm{d}\mathbf{x} \\ &\quad - \oiint_{\delta\Omega} \chi(\mathbf{x}) (\vec{\mathbf{n}} \cdot \nabla)(\nabla' G(\mathbf{p},\mathbf{x})) \mathrm{d}\mathbf{x} \end{aligned} \tag{48}$$

Since the integrands are irrotational and solenoidal, so is their superposition by the integral. If function χ takes a constant value on the surface of the obstacle, say 0, then $\nabla\chi$ is aligned with $\vec{\mathbf{n}}$ and we can impose the Neumann boundary condition $\vec{\mathbf{v}} + \vec{\mathbf{h}}_{\Omega^c} = 0$ on $\delta\Omega$. Note that if surface $\delta\Omega$ is topologically not simply connected, then χ is only locally defined, but since we set χ to 0 on the boundary, we can reconnect the branches of χ.

D Boundary Vorticity

The vorticity near the boundary Ω of a moving object is given by $\nabla \log(\rho) \times (\vec{\mathbf{F}} - \vec{\mathbf{a}}) + \nabla \times \vec{\mathbf{F}}$, where $\vec{\mathbf{a}}$ is the acceleration near the boundary. To compute this term, we consider a coordinate system where the half space $z < 0$ is inside the solid object, $z = 0$ is on the object's surface, and $z > 0$ is outside. Using the Heaviside step function H, the nearby density is formally defined as $\rho = \mathrm{H}(-z)\rho_0 + \mathrm{H}(z)\rho_1$, the external forces term is defined as $\vec{\mathbf{F}} = \mathrm{H}(-z)\vec{\mathbf{f}} + \mathrm{H}(z)(\vec{\mathbf{g}} + \vec{\mathbf{e}})$, and the acceleration is $\vec{\mathbf{a}} = \mathrm{H}(-z)\vec{\mathbf{f}} + \mathrm{H}(z)\frac{\mathrm{d}\vec{\mathbf{v}}}{\mathrm{d}t}$. Since we solve for vorticity, we can replace $\vec{\mathbf{F}}$ with any $\vec{\mathbf{F}} + \vec{\mathbf{G}}$ to satisfy the boundary condition as long as $\nabla \times \vec{\mathbf{G}} = 0$ in Ω^c. First let us consider the following $\vec{\mathbf{G}}$

$$\vec{\mathbf{G}} = \mathrm{H}(z)\left(\frac{\mathrm{d}\vec{\mathbf{v}}}{\mathrm{d}t} - \vec{\mathbf{g}} - \frac{1}{2}\vec{\mathbf{e}}\right) - \frac{1}{2}\vec{\mathbf{e}} \tag{49}$$

Although $\frac{\mathrm{d}\vec{\mathbf{v}}}{\mathrm{d}t}$ may have curl, we discretize the object surface in regions of constant $\frac{\mathrm{d}\vec{\mathbf{v}}}{\mathrm{d}t}$. To prevent the space inside objects from contributing to the non-rigid fluid motion, we set $\rho_0 \to \infty$, thus enforcing $\vec{\mathbf{f}}$ inside objects. We take the limit of the integral of the collision term near the surface using the following limit to the heavyside step function $\mathrm{H}(z) = \lim_{t\to\infty} \frac{1}{2} + \frac{1}{\pi}\tan^{-1}(zt)$, and obtain the surface vorticity

$$\begin{aligned} &\lim_{\rho_0\to\infty}\lim_{t\to\infty}\int_{-h}^{h} \nabla\log(\rho) \times \left(\vec{\mathbf{F}} + \vec{\mathbf{G}} - \tfrac{\mathrm{d}\vec{\mathbf{v}}}{\mathrm{d}t}\right) + \\ &\qquad \nabla \times (\vec{\mathbf{F}} + \vec{\mathbf{G}})\,\mathrm{d}z \\ &= (\vec{\mathbf{f}} - \vec{\mathbf{e}} - \vec{\mathbf{a}}) \times \vec{\mathbf{n}} \end{aligned} \tag{50}$$

References

ANGELIDIS, A., NEYRET, F., SINGH, K., AND NOWROUZEZAHRAI, D. 2006. A controllable, fast and stable basis for vortex based smoke simulation. In *Proceedings of the 2006 ACM SIGGRAPH/Eurographics Symposium on Computer Animation*, Eurographics Association, SCA '06, 25–32.

ARIS, R. 2012. *Vectors, Tensors and the Basic Equations of Fluid Mechanics*. Dover Books on Mathematics. Dover Publications.

COTTET, G.-H., AND KOUMOUTSAKOS, P. D. 2000. *Vortex Methods: Theory and Practice*. Cambridge University Press.

DE WITT, T., LESSIG, C., AND FIUME, E. 2012. Fluid simulation using Laplacian eigenfunctions. *ACM Trans. Graph. 31*, 1 (Feb.), 10:1–10:11.

DECAUDIN, P. 1996. Geometric deformation by merging a 3D object with a simple shape. In *Graphics Interface*, 55.

DESBRUN, M., AND GASCUEL, M.-P. 1996. Smoothed particles: A new paradigm for animating highly deformable bodies. In *Proceedings of the Eurographics Workshop on Computer Animation and Simulation '96*, Springer-Verlag New York, Inc., 61–76.

ELCOTT, S., TONG, Y., KANSO, E., SCHRÖDER, P., AND DESBRUN, M. 2007. Stable, circulation-preserving, simplicial fluids. *ACM Trans. Graph. 26*, 1 (Jan.).

FOSTER, N., AND METAXAS, D. 1997. Modeling the motion of a hot, turbulent gas. In *Proceedings of the 24th Annual Conference on Computer Graphics and Interactive Techniques*, ACM Press/Addison-Wesley Publishing Co., SIGGRAPH '97, 181–188.

FRISCH, U., AND KOLMOGOROV, A. 1995. *Turbulence: The Legacy of A. N. Kolmogorov*. Turbulence: The Legacy of A.N. Kolmogorov. Cambridge University Press.

GIBOU, F., AND MIN, C. 2012. On the performance of a simple parallel implementation of the ilu-pcg for the Poisson equation on irregular domains. *Journal of Computational Physics*.

KIM, T., THÜREY, N., JAMES, D., AND GROSS, M. 2008. Wavelet turbulence for fluid simulation. *ACM Trans. Graph. 27*, 3 (Aug.), 50:1–50:6.

MCADAMS, A., SIFAKIS, E., AND TERAN, J. 2010. A parallel multigrid Poisson solver for fluids simulation on large grids. In *Proceedings of the 2010 ACM SIGGRAPH/Eurographics Symposium on Computer Animation*, Eurographics Association, SCA '10, 65–74.

PARK, S. I., AND KIM, M. J. 2005. Vortex fluid for gaseous phenomena. In *Proceedings of the 2005 ACM SIGGRAPH/Eurographics Symposium on Computer Animation*, ACM, SCA '05, 261–270.

PFAFF, T., THUEREY, N., AND GROSS, M. 2012. Lagrangian vortex sheets for animating fluids. *ACM Trans. Graph. 31*, 4 (July), 112:1–112:8.

SELLE, A., RASMUSSEN, N., AND FEDKIW, R. 2005. A vortex particle method for smoke, water and explosions. In *ACM SIGGRAPH 2005 Papers*, ACM, SIGGRAPH '05, 910–914.

STAM, J. 1999. Stable fluids. In *Proceedings of the 26th Annual Conference on Computer Graphics and Interactive Techniques*, ACM Press/Addison-Wesley Publishing Co., SIGGRAPH '99, 121–128.

ZHANG, X., AND BRIDSON, R. 2014. A PPPM fast summation method for fluids and beyond. *ACM Trans. Graph. 33*, 6 (Nov).